Time-resolved Z-scan measurements of optical nonlinearities

J. Wang, M. Sheik-Bahae, A. A. Said, D. J. Hagan, and E. W. Van Stryland

Center for Research in Electro-Optics and Lasers, University of Central Florida, Orlando, Florida 32816

Received September 17, 1993; revised manuscript received January 28, 1994

We introduce a temporal delay in one beam of the two-color Z-scan apparatus, which measures nondegenerate nonlinear absorption and nondegenerate nonlinear refraction. This technique allows us to time resolve separately the sign and the magnitude of the nonlinear absorption and refraction at frequency ω_p that are due to the presence of a strong excitation at frequency ω_e. For example, in semiconductors we specifically measure the bound electronic, nondegenerate nonlinear refraction and nondegenerate two-photon absorption, as well as the two-photon-generated free-carrier refraction and absorption as functions of time. We demonstrate this technique on ZnSe, ZnS, and CS_2, using picosecond pulses at 1.06 and 0.532 μm.

1. INTRODUCTION

Interpretations of measurements of optical nonlinearities of materials are often complicated by the presence or the competition of two or more nonlinear mechanisms. In many cases the experimental technique cannot distinguish between these different nonlinearities. For example, the degenerate four-wave mixing (DFWM) signal for a cubic nonlinearity is proportional to $|\chi^{(3)}|^2$, where $\chi^{(3)}$ is the third-order susceptibility.[1] Index changes $\{\mathrm{Re}[\chi^{(3)}]\}$ and losses $\{\mathrm{Im}[\chi^{(3)}]\}$ both contribute to the DFWM signal; therefore they are indistinguishable in DFWM experiments. A further complication can arise from contributions of ultrafast and cumulative nonlinearities. For example, in semiconductors we have observed the simultaneous presence of the bound electronic optical Kerr effect (ultrafast n_2) and two-photon absorption (2PA), along with free-carrier absorption and refraction, which are cumulative for decay times longer than the pulse width.[2,3] In this paper we present a technique for unraveling the various contributions to the nonlinear response of a material. We demonstrate this technique, which is a time-resolved two-color Z scan,[4,5] for separating the nonlinearities occurring in ZnSe, ZnS, and CS_2 when these materials are irradiated by picosecond pulses at 1.06 and 0.532 μm.

The two-color Z scan[4,5] measures the nondegenerate nonlinear response of a material at the probe frequency ω_p that is due to the presence of an excitation beam at frequency ω_e. This method is capable of separating the refractive and the absorptive nonlinear contributions but cannot distinguish between ultrafast and cumulative nonlinearities. The introduction of a temporal delay into the two-color Z-scan apparatus permits separation of the nonlinearities having a different temporal response.

We first describe the experimental arrangement and its calibration. An example of time-resolved data for CS_2 displaying only nonlinear refraction is given, followed by results on ZnSe and ZnS. The semiconductor data give values for the nondegenerate Kerr effect $n_2(\omega_p; \omega_e)$, including the sign and the magnitude, the nondegenerate 2PA coefficient $\beta(\omega_p; \omega_e)$, and the free-carrier refractive coefficient $\sigma_r(\omega_p)$ and absorptive cross section $\sigma_a(\omega_p)$.

2. EXPERIMENTAL ARRANGEMENT

The experimental arrangement, shown in Fig. 1, is an extension of the Z-scan arrangement of Refs. 6 and 7. The extracted 43-ps (FWHM) pulse from a Q-switched and mode-locked Nd:YAG laser (λ = 1.06 μm) is separated into two beams by a variable beam splitter that controls the irradiance ratio between them. One of the beams passes through a variable time-delay stage while the second goes through a second-harmonic-generating crystal to produce 0.532-μm light. The polarization of the beams is separately controlled by half-wave plates. The two beams are recombined by a dichroic beam splitter and are focused with a nearly achromatic lens of focal length f = 15 cm onto the sample. A second dichroic beam splitter then separates the two beams for detection after passing through apertures of transmittance S.

In this time-resolved two-color Z-scan experimental setup, the sample position Z, with respect to the probe-beam waist and the time delay t_d between the excitation and the probe beams, is independently varied according to the experiment, as described below. The measured quantity is the normalized transmittance as a function of Z (Z scan) or as a function of t_d (temporal scan). Analogous to the usual single-wavelength Z scan, an open-aperture (S= 1, i.e, no aperture) Z scan at a fixed delay is sensitive only to the induced changes in absorption, whereas a closed-aperture (i.e, partially closed aperture) Z scan displays the induced refractive changes as well. We use an aperture of S = 0.4 for all closed-aperture data given in this paper. In the absence of nonlinear absorption, the change in transmittance between the peak (transmittance maximum) and the valley (transmittance minimum) in a closed-aperture Z scan, defined as ΔT_{pv}, is linearly proportional to the induced phase distortion,

0740-3224/94/061009-09$06.00

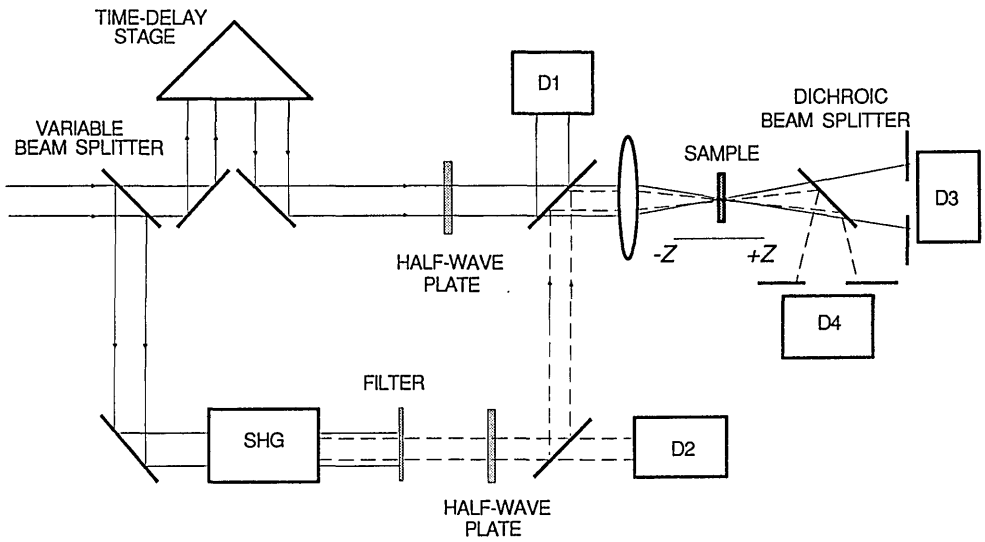

Fig. 1. Time-resolved excite–probe two-color Z-scan experimental apparatus. D1–D4, detectors. SHG, second-harmonic-generating crystal.

which in turn is proportional to the nondegenerate nonlinear refractive index. When nonlinear absorption is also present, as discussed in Ref. 7, the division of closed-aperture data by open-aperture data again gives the nonlinear refraction, as long as the nonlinear absorption is not too large (the same criterion as is discussed in Ref. 7 is valid here). We refer to the results of this division as a divided Z scan. If we measure the transmittance as a function of time delay for a fixed sample position, we can separately determine the dynamics of the nonlinear absorption (open aperture) and refraction (closed aperture). If the time-delay stage is fixed at long time delays such that there is no overlap between probe and excitation, the Z scan is sensitive only to long-lived nonlinearities, which in semiconductors provides an independent measurement of free-carrier absorption and refraction, separated from the bound electronic nonlinearities.

To determine the temporal response of the nonlinear absorption and refraction, we use the following procedure: Zero temporal delay is first determined in the manner discussed toward the end of this section. We then place the sample at the minimum transmittance position of an open-aperture Z scan (i.e., at the position of the waist). The temporal delay is then scanned to measure the normalized transmittance as a function of time delay t_d. We refer to this open-aperture transmittance as $T_{op}(t_d)$, and it gives the nonlinear absorption as a function of time. Measurement of the nonlinear refraction is somewhat more complicated but is based on the linear relation between ΔT_{pv} and the phase distortion.

For materials showing no degenerate or nondegenerate nonlinear absorption, a closed-aperture Z scan at a fixed time delay is used to determine the transmittance peak and valley Z positions. With the sample fixed at the position of the peak, we scan the time-delay stage. This procedure is repeated with the sample placed at the Z position of the valley. The difference between these two sets of data is $\Delta T_{pv}(t_d)$, which is directly proportional to the nonlinear-induced phase change. For the time delay fixed at $t_d = 0$, this phase change is proportional to the nondegenerate nonlinear refractive index $n_2(\omega_p; \omega_e)$. If both nonlinear absorption and nondegenerate nonlinear refraction are present, both open- and closed-aperture temporal scans must be performed at the position of the peak and the valley for the divided Z scan. The temporal-scan results are then divided to obtain $\Delta T_{pv}(t_d)$ (one can perform these scans simultaneously by using a beam splitter in the transmitted probe beam and the two detectors, one without and one with an aperture). As long as the nondegenerate nonlinear absorption remains small, $n_2(\omega_p; \omega_e)$ remains proportional to ΔT_{pv}.[7] In general any two frequencies can be used as long as the beams can be spatially and temporally overlapped. This technique can also be used for two beams having the same wavelength; however, the experiment becomes more difficult because of coherent interactions, which require interferometric stability for interpretation. However, the use of counterpropagating beams would permit separation of the beams but would add complexity to temporal-delay measurements.

In the experiments presented here, we can use either the fundamental (1.06-μm) or the second-harmonic (0.532-μm) beam as the excitation. We absolutely calibrate the pulse widths and the beam waists of the two Gaussian beams. This necessitates performing spatial beam scans and temporal autocorrelations of both the fundamental and the second-harmonic beams, as well as determining the longitudinal separation between the two beam waists caused by residual chromatic aberration of the focusing lens. By performing single-wavelength closed-aperture Z scans at 1.06 and 0.532 μm on a 1-mm cell containing CS_2, we determined that the beam waists were separated by 1.5 mm because of chromatic aberration in the lens. Such aberration is easily accounted for in the numerical fitting routine described in Section 4. Additionally, as the separation between the peak and the valley of the transmittance (ΔZ_{pv}) for a third-order response is $\simeq$1.7 times the Rayleigh range, this measurement confirmed that the spot sizes at focus (half-width at $1/e^2$ maximum in irradiance) were 27 and 20 μm for the 1.06- and the 0.532-μm beams, respectively. Using autocorrelation measurements, we determined the pulse

widths (FWHM) to be 43 and 31 ps at 1.06 and 0.532 μm, respectively. The estimated uncertainty in the spot-size and the pulse-width measurements are $\pm 5\%$. The incident and the transmitted pulse energies are detected by integrating silicon photodiodes. A spike filter at the appropriate wavelength is placed in front of each detector. Each data point is an average of 10 shots, taken with the aid of an automated data-acquisition system. While the Z-scan data are acquired, the pulse width and energy are also monitored, and acceptance windows of $\pm 5\%$ are set for both pulse width and input energy to increase the signal-to-noise ratio.[8] The absolute irradiances at the sample for each beam can then be calculated given the energy as calibrated by a pyroelectric energy meter.

A limitation of this method is the range of temporal delays that can be scanned while the position of focus and the waist size of the delayed beam are kept constant. We maximized this range by minimizing the divergence of the laser beams before the focusing lens. We used a measured input beam divergence of 3.4×10^{-4} rad, and we calculate for our geometry ($\simeq$2 m from the waist) that a 1-ns time delay changes the waist size by $\simeq 4\%$ at 1.06 μm. This delay also results in a displacement of the focus that is negligible ($<1\%$ of f).

For the two-color experiment, maintaining the spatial overlap around focus is crucial. A 6-arcsec angle between the two beams as they enter the focusing lens would give a 10% offset of the spatial overlap of the two beams at focus ($\Delta x \simeq 2$ μm for a beam waist of 20 μm). Prior to inserting the focusing lens, we propagate the two beams for $\simeq$4 m and ensure their spatial overlap by maximizing the transmittances through apertures. A similar procedure is repeated near the focus once the focusing lens is inserted. Finally, we achieve a fine adjustment of the spatial overlap at focus by maximizing the change in transmittance of the probe, using a nonlinear absorber. The change in the probe transmittance is maximized when the two Gaussian beams are overlapped (i.e., their on-axis points are coincident). The nonlinear absorber used in this technique may be a nondegenerate two-photon absorber, an excited-state absorber, or a saturable absorber; however, because the 2PA process is nearly instantaneous, it requires temporal overlap of the laser pulses as well. Therefore an excited-state or a saturable absorbing medium with a long recovery time is easier to use initially.

After ensuring spatial overlap, it is necessary to determine the position of zero time delay between the excitation and the probe beams. Performing a closed-aperture time scan on CS_2 with the sample stage positioned near the Z-scan peak, we obtain the data shown in Fig. 2. This procedure gives the temporal cross-correlation function between the two beams, provided that the transmittance through the aperture varies linearly with the excitation irradiance. This result is valid as long as ΔT_{pv} is linearly dependent on the excitation, i.e., for transmittance changes to as much as $\simeq 20\%$ when the sample is placed at the peak or the valley.[7] Returning to Fig. 2, we find that the width of 53 ps (FWHM) for this curve agrees with a calculation of the cross correlation for the pulses of FWHM 43 and 31 ps at 1.06 and 0.532 μm, respectively, as measured by the individual second-order autocorrelation functions. Hence we have shown that the two-color Z scan can be used as a cross correlator to measure pulse widths, provided that one of the pulse widths is known or, as in the case of harmonic or parametric processes, that a fixed relationship between the two pulses exist. Like any nonlinear correlation technique, the temporal resolution of this technique is limited by the response time of the nonlinearity. For UV pulses for which second-harmonic-generating crystals are not available, this method may prove useful.

3. THEORY

A. Semiconductor Nonlinearities

In the picosecond regime optical nonlinearities in semiconductors under nonresonant excitation (i.e., in the transparency regime) are generally a combination of bound electronic and free-carrier effects. Bound electronic nonlinearities arising from an anharmonic response of the valence electrons are ultrafast, with a typical response time being of the order of an optical cycle. This process can be regarded as instantaneous when laser pulses containing many optical cycles are used. We characterize this response with $\chi^{(3)}$. In the transparency regime free-carrier nonlinearities rely on multiphoton carrier generation and appear as higher-order phenomena. In particular, free-carrier refraction and absorption that are due to charge carriers generated by 2PA can be characterized as an effective $\chi^{(5)}$ process.[3] Most importantly, free-carrier effects are further distinguishable from the bound electronic effect because of their long recovery time determined by the free-carrier lifetime.[9] A time-resolved study of these processes can therefore identify and characterize the various contributions.

We define the total change of refractive index (Δn) and absorption coefficient ($\Delta\alpha$) as the sum of the bound electronic (subscript b) and free-carrier (subscript f) contributions:

$$\Delta n(\omega_p; \omega_e) = \Delta n_b + \Delta n_f, \tag{1a}$$

$$\Delta \alpha(\omega_p; \omega_e) = \Delta \alpha_b + \Delta \alpha_f. \tag{1b}$$

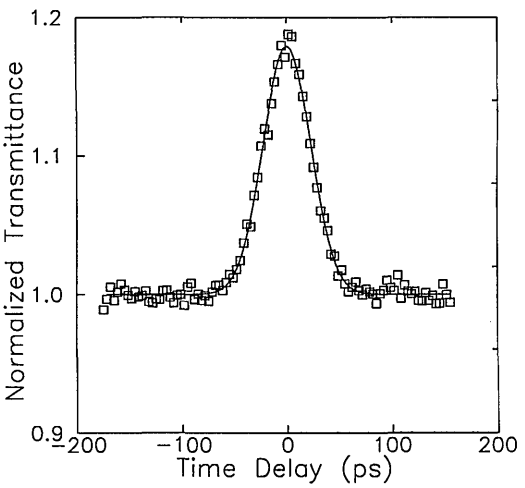

Fig. 2. Time-resolved two-color Z scan of CS_2 obtained with $\lambda = 1.06$ μm as the excitation and $\lambda = 0.532$ μm as the probe. This procedure gives the cross correlation of these two pulses and determines the zero-time-delay position.

The quantities for describing the bound electronic effect are the nonlinear refractive index $n_2(\omega_p;\ \omega_e)$ and the 2PA coefficient $\beta(\omega_p;\omega_e)$ measured at probe frequency ω_p that are due to the presence of the excitation beam at frequency ω_e. We define these coefficients as

$$\Delta n_b(\omega_p;\omega_e) = 2n_2(\omega_p;\omega_e)I_e, \tag{2a}$$

$$\Delta\alpha_b(\omega_p;\omega_e) = 2\beta(\omega_p;\omega_e)I_e, \tag{2b}$$

where I_e is the irradiance of the excitation beam. The factor of 2 comes from weak-wave retardation.[5,10] The coefficients n_2 and β are related through Kramers–Kronig dispersion relations by virtue of the principle of causality.[11–14] Recently the Kramers–Kronig relations were employed to calculate the dispersion and the band-gap scaling of n_2 in solids from the calculated nonlinear absorption spectrum (including 2PA) by use of a simple two-parabolic-band model.[12] The degenerate n_2 and β measured with single-beam Z scans strongly support this theory. Because the nonlinear Kramers–Kronig relation generally relates the nondegenerate nonlinear absorption with the nondegenerate nonlinear refraction, the two-color Z scan provides a direct comparison with this theory.[5]

The induced free-carrier refraction and absorption naturally depend on the density of photogenerated carriers (ΔN) produced by 2PA when it is energetically allowed. For most cases in which the probe photon energy is far enough from the band edge (i.e., the index change is small enough), it is sufficient to assume a linear dependence on ΔN, giving[9,15–17]

$$\Delta n_f(\omega_p;\omega_e) = \sigma_r(\omega_p)\Delta N(t), \tag{3a}$$

$$\Delta\alpha_f(\omega_p;\omega_e) = \sigma_a(\omega_p)\Delta N(t), \tag{3b}$$

where the time dependence of ΔN is explicitly shown. Here σ_r (in cubic centimeters) denotes the change of refractive index per unit carrier density, whereas σ_a (in square centimeters) is known as the free-carrier absorption cross section. In these experiments the probe is weak compared with the excitation beam, so we consider degenerate 2PA of the excitation beam as the only source of carrier generation. Thus the carrier-generation rate is given by

$$\frac{d\Delta N}{dt} = \frac{\beta(\omega_e;\omega_e)}{2\hbar\omega_e} I_e{}^2 - \frac{\Delta N}{\tau_r}, \tag{4}$$

where τ_r is the carrier lifetime. Here we assume a quasi-equilibrium condition in which the 2PA-generated carriers in the conduction band have thermalized with the lattice. For the pulse widths used in our experiments this is a valid assumption because electron–phonon scattering ensures the quasi-equilibrium condition within 1–2 ps.[18] The mechanism for free-carrier refraction is a combination of plasma and band-filling effects[2,15–17] with a lifetime τ_r typically of the order of nanoseconds.[9] On the other hand, free-carrier absorption in most semiconductors originates from heavy-hole to light-hole intervalence band absorption and is usually weak unless it is probed at longer wavelengths, i.e., in the mid or the far IR.[19]

B. Propagation

By invoking the slowly varying envelope approximation and the thin-sample approximation,[20] we can reduce the Maxwell equations to obtain separate equations governing the amplitude ($|E_p|$) and the phase (ϕ_p) of the probe beam:

$$2\frac{\partial|E_p|}{\partial z'} + \alpha_p|E_p| = -2\beta(\omega_p;\omega_e)|E_p|I_e - \sigma_a(\omega_p)\Delta N|E_p|, \tag{5a}$$

$$\frac{\partial\phi_p}{\partial z'} = \frac{\omega_p}{c}2n_2(\omega_p;\omega_e)I_e + \sigma_r(\omega_p)\Delta N. \tag{5b}$$

The depletion of the excitation beam is given by

$$\frac{\partial I_e}{\partial z'} + \alpha_e I_e = -\beta(\omega_e;\omega_e)I_e{}^2, \tag{6}$$

where α_p and α_e are the linear absorption coefficients of the probe and the excitation beams, respectively. For a given sample position Z, the incident slowly varying field amplitude E_p and I_e (at $z' = 0$) are taken to have the well-known Gaussian beam functional dependence radially as well as temporally[21]:

$$E_p(z'=0) = E_{0p}\frac{w_{0p}}{w_p}\exp\left[-\frac{r^2}{w_p{}^2}\left(1+\frac{iZ}{Z_{0p}}\right)-\frac{t^2}{2\tau_p{}^2}\right]\times\exp\left[-i\tan^{-1}\left(\frac{Z}{Z_{0p}}\right)\right], \tag{7}$$

$$I_e(z'=0) = I_{0e}\frac{w_{0e}{}^2}{w_e{}^2}\exp\left[-\frac{2r^2}{w_e{}^2}-\frac{(t-t_d)^2}{\tau_e{}^2}\right], \tag{8}$$

where $w_p{}^2 = w_{0p}{}^2[1 + (Z^2/Z_{0p}{}^2)]$ and $w_e{}^2 = w_{0e}{}^2\{1 + (Z + Z_c)^2/Z_{0e}{}^2]\}$ define the probe- and the excitation-beam radii (half-width at $1/e^2$ maximum in irradiance), respectively, with Z_c accounting for the axial shift of the two foci that are due to the chromatic aberration of the focusing lens. The nonradial-dependent phase shift in Eq. (7) is unimportant in these experiments and is henceforth ignored. $Z_{0j} = \pi w_{0j}{}^2/\lambda_j$, where ($j = p, e$), are the Rayleigh ranges, and τ_p and τ_e denote the half-width at $1/e$ pulse widths (in irradiance) of probe and excitation beams, respectively.

A simultaneous solution to Eqs. (4)–(6) that uses the initial condition imposed by Eqs. (7) and (8) gives the radial (r dependence) and the temporal variations of $|E_p|$, ϕ_p, and I_e after propagation through the sample of thickness L for a fixed sample position Z. Once the amplitude and the phase of the probe are determined at the exit surface of the sample, we can obtain the probe beam's profile at the aperture plane ($\mathbf{E}_a$) by applying the Huygen–Fresnel principle through a Hankel transformation of E_p evaluated at $z' = L$.[22] This yields

$$E_a(r,t,Z) = \frac{2\pi}{i\lambda_p(d-Z)}\exp\left[\frac{i\pi r^2}{\lambda_p(d-Z)}\right]\times\int_0^\infty r'dr'E_p(r',t,Z,z'=L)\times\exp\left[\frac{i\pi r'^2}{\lambda_p(d-Z)}\right]J_0\left[\frac{2\pi rr'}{\lambda_p(d-Z)}\right], \tag{9}$$

where d is the distance between the position of the focal point of the excitation beam and the aperture plane and J_0 is the Bessel function of zeroth order. The normalized transmittance is given by

$$T(t_d, Z) = \frac{\int_{-\infty}^{\infty} dt \int_0^{r_a} r dr |E_a|^2}{\int_{-\infty}^{\infty} dt \int_0^{r_a} r dr |E_a(I_e = 0)|^2}, \qquad (10)$$

where r_a is the aperture radius that for an open-aperture Z scan is infinite. It is more convenient to specify the aperture transmittance $S = 1 - \exp(-2r_a^2/w_a^2)$, where w_a is the beam radius at the aperture in the linear regime. Under certain conditions Eqs. (4)–(10) can be solved analytically, but in general a numerical solution is required.[23] In the analysis of time-resolved data, the quantities ΔT_{pv} and T_{op}, as a function of the time delay t_d, are calculated with Eq. (10):

$$\Delta T_{pv}(t_d) = \pm\left[\frac{T(t_d, Z_p)}{T_{op}(t_d, Z_p)} - \frac{T(t_d, Z_v)}{T_{op}(t_d, Z_v)}\right] \quad \text{for } S < 1,$$
$$T_{op}(t_d) = T(t_d, 0) \quad \text{with } S = 1, \qquad (11)$$

where Z_p and Z_v are the positions of peak and valley of the Z scan, respectively. The sign of ΔT_{pv} is given by the sign of $Z_p - Z_v$.

As discussed in Section 4, the spatial separation between peak and valley, ΔT_{pv}, depends on the order of the nonlinearity equaling $\simeq 1.7 z_0$ for a third-order response and $\simeq 1.2 z_0$ for a fifth-order nonlinearity. Thus, in performing a temporal scan, one can optimize the signal for a third- or a fifth-order nonlinearity, although the difference in signal is only approximately 20%. This must be accounted for in interpreting the results of a temporal scan when both types of nonlinearity are present.

4. RESULTS AND DISCUSSION

The semiconductor samples used in our experiments are zinc blende polycrystalline slabs of ZnSe and Cleartran ZnS. ZnSe has a band-gap energy of $E_g = 2.6$ eV,[24] $n_0 = 2.5$ at $\lambda = 1$ μm, and $n_0 = 2.7$ at $\lambda = 0.5$ μm. The sample thickness is 2.7 mm. The ZnS sample has a thickness of 1 mm, $E_g = 3.7$ eV,[24] $n_0 = 2.3$ at 1 μm, and $n_0 = 2.4$ at 0.5 μm. In the following discussion, ω refers to 1.06-μm light and 2ω to 0.532-μm light. Table 1 summarizes the results described below.

A. Excitation at 1.06 μm

In both ZnSe and ZnS, degenerate 2PA with $\lambda_p = 1.06$ μm is energetically forbidden (i.e., $2\hbar\omega < E_g$). Therefore, with the strong excitation beam at 1.06 μm, the free-carrier density (ΔN) remains small, and the induced Δn and $\Delta\alpha$ are dominated by ultrafast bound electronic effects. However, in experiments on both polycrystalline ZnSe and ZnS, scattered second-harmonic light at 532 nm could be seen. Hence care was taken to ensure that second-order effects[25] did not influence our results. In ZnSe the probe at $\lambda_p = 532$ nm experiences a nondegenerate 2PA because $\hbar\omega + 2\hbar\omega = 3.5$ eV exceeds the band-gap energy of ZnSe. The open-aperture and closed-aperture Z-scan data at zero temporal delay, obtained with an excitation irradiance (I_e) of 0.7 GW/cm^2, are shown in Fig. 3. Measurements were made for two cases of parallel-polarized (xx) and crossed-polarized (xy) excitation and probe beams. From the calculations, the best fits give $\beta^{xx}2(\omega;\omega) = 15 \pm 3$ cm/GW, $\beta^{xx}(2\omega;\omega/\beta^{xy}(2\omega;\omega) = 1.7 \pm 0.4$, $n_2{}^{xx}(2\omega;\omega) = -(5.1 \pm 1.0) \times 10^{-14}$ cm^2/W, and $n_2{}^{xx}(2\omega;\omega)/n_2{}^{xy}(2\omega;\omega) = 2.0 \pm 0.5$ (see Table 1). All the results in Table 1 refer to parallel polarization unless specifically noted with the superscript xy. The observed polarization dichroism has been attributed to the interference between contributions to $\chi^{(3)}$ from the heavy-hole and the light-hole valence bands.[26]

For ZnS with $\hbar\omega + 2\hbar\omega < E_g$, nondegenerate 2PA is not permitted, and the measured nonlinearities are purely refractive (degenerate 2PA for the probe at 532 nm is weak). Figure 4 shows the

Table 1. Nondegenerate Nonlinear Parameters Extracted from the Time-Resolved Two-Color Z-Scan Data[a]

Parameter	Material: ZnSe	Material: ZnS
β (1.06;1.06)	0	0
β (0.532;0.532)	5.8 ± 1 cm/GW	3.4 ± 0.7 cm/GW
β (0.532;1.06)	15 ± 3 cm/GW	0
β (1.06;0.532)	4.6 ± 1 cm/GW	0
β^{xy} (1.06;0.532)	8.6 ± 2 cm/GW	0
n_2 (1.06;1.06)	$(2.9 \pm 0.3) \times 10^{-14}$ cm^2/W	$(6.3 \pm 1.4) \times 10^{-15}$ cm^2/W
n_2 (0.532;0.532)	$(-6.8 \pm 1.4) \times 10^{-14}$ cm^2/W	Not measured
n_2 (0.532;1.06)	$(-5.1 \pm 0.5) \times 10^{-15}$ cm^2/W	$(1.7 \pm 0.4) \times 10^{-14}$ cm^2/W
$n_2{}^{xy}$ (0.532;1.06)	$(-2.6 \pm 0.3) \times 10^{-14}$ cm^2/W	Not measured
n_2 (1.06;0.532)	$(-9 \pm 5) \times 10^{-15}$ cm^2/W	$<1.5 \times 10^{-14}$ cm^2/W
σ_a (1.06)	$(4.4 \pm 1.3) \times 10^{-18}$ cm^2	$(7 \pm 2) \times 10^{-18}$ cm^2
σ_r (1.06)	$(-6.1 \pm 1.5) \times 10^{-22}$ cm^3	$(5.2 \pm 1.1) \times 10^{-22}$ cm^3
τ	$\approx$1 ns	$\tau_a \approx 0.6$ ns; $\tau_r \approx 0.8$ ns

[a] β, 2PA coefficient; n_2 bound electronic nonlinear refractive index; σ_a, free-carrier absorptive cross section; σ_r, free-carrier refractive coefficient.

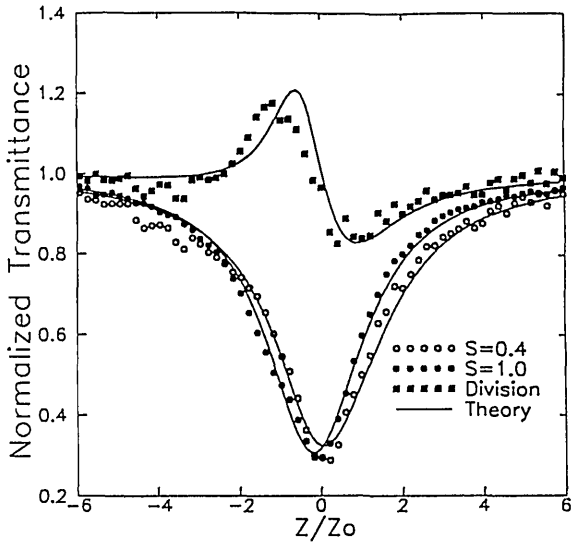

Fig. 3. Open-aperture data (filled circles) and closed-aperture data (open circles) for ZnSe obtained with perpendicularly polarized beams at zero time delay (excitation at 1.06 μm and probe at 0.532 μm). The squares show the division of the two data sets, and the curves represent theoretical fits.

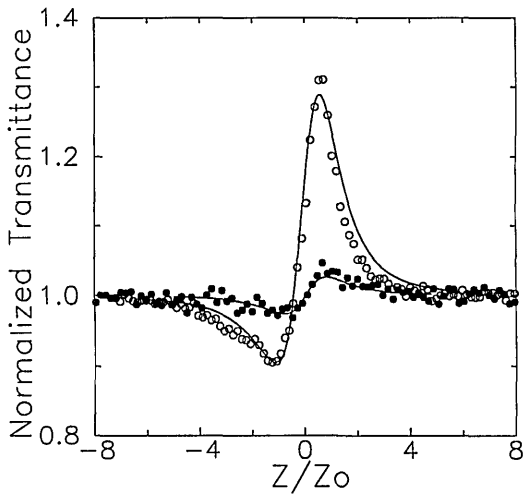

Fig. 4. Closed-aperture degenerate Z-scan data (filled circles) and closed-aperture nondegenerate data (open circles) obtained with excitation at 1.06 μm and probe at 0.532 μm for ZnS obtained with parallel-polarized beams at zero time delay. The curves represent theoretical fits.

closed-aperture Z-scan signal compared with the single-wavelength Z scan at 1.06 μm measured at $I_e \simeq 8.5$ GW/cm^2. The best fit to these data gives a ratio of $n_2(2\omega;\omega)/n_2(\omega;\omega) \simeq 1.9 \pm 0.2$ for parallel-polarized beams, with $n_2(\omega;\omega) = (7.6 \pm 1.5) \times 10^{-15}$ cm^2/W. This large ratio is due to a two-photon resonant enhancement of $n_2(\omega;\omega)$.[27] The theoretical analysis regarding the observed dispersion of the nondegenerate n_2 is given in Ref. 12. There is only an ultrafast response at this excitation wavelength, at which 2PA is not permitted.

B. Excitation at 0.532 μm

With excitation at 0.532 μm during probing at 1.06 μm, degenerate 2PA of the pump beam is present in both ZnSe and ZnS. We employ this arrangement primarily to study the induced free-carrier nonlinearities. By performing a temporal scan in the two-color Z-scan experiment, we can differentiate the free-carrier nonlinearities from the bound electronic effects. We use the method discussed in Section 2 to separate absorptive and refractive nonlinearities.

For ZnSe, $\Delta T_{pv}(t_d)$ and the maximum open-aperture transmittance change $\Delta T_{op}(t_d)$ are measured for several different input irradiances. As mentioned above, the signal can be optimized for either the third- or the fifth-order response. Here (as was done for the data given in Fig. 5), we optimized the signal for the fifth-order response of the carrier nonlinearities by first performing a Z scan at a long delay (i.e., $t_d \gg t_p$) to find the position of peak and valley. This means that the fast-response

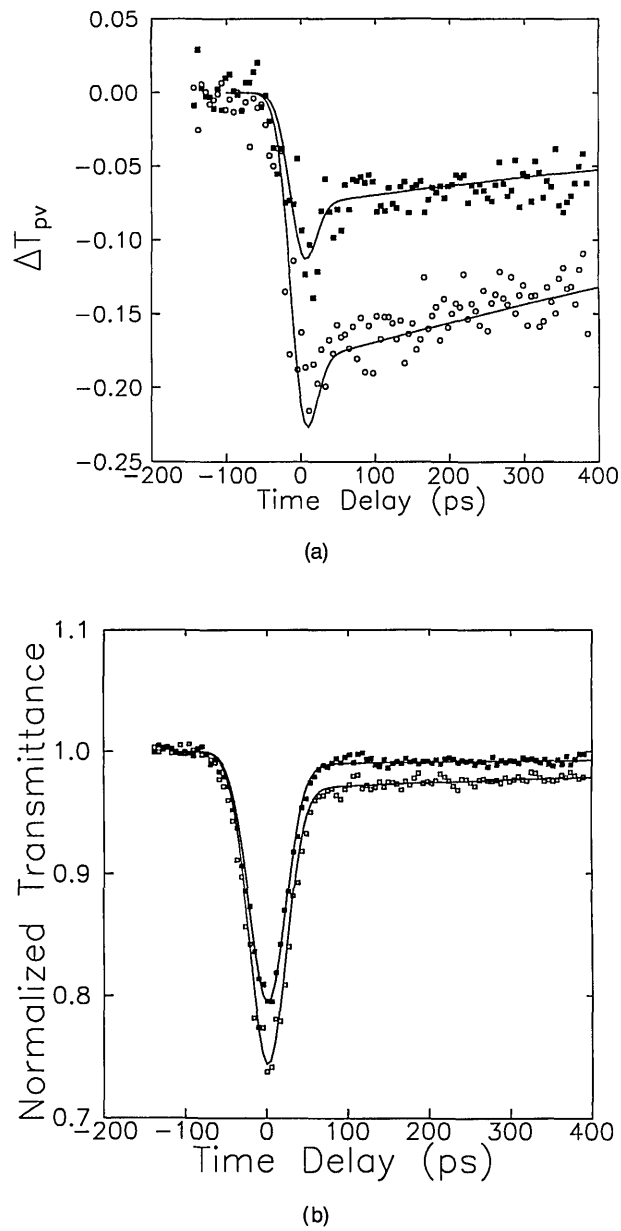

Fig. 5. (a) Nonlinear refraction as determined by $\Delta T_{pv}(t_d)$ and (b) nonlinear absorption from the normalized transmittance $T_{op}(t_d)$ as a function of probe-beam time delay t_d for ZnSe measured at $I_e = 1.2$ GW/cm^2 (open symbols) and $I_e = 0.7$ GW/cm^2 (filled squares). $\tau_r = 1$ ns. The curves are fits to the data obtained with the values given in Table 1.

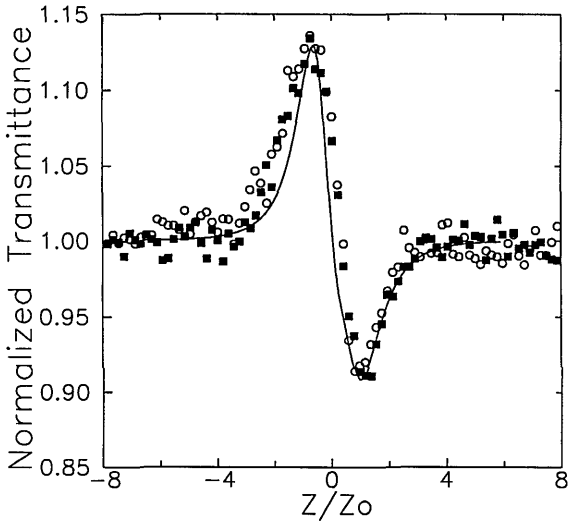

Fig. 6. Nondegenerate divided Z scans on ZnSe at time delays of 100 ps (circles) and 200 ps (squares) obtained with 0.53 μm as the excitation source and 1.06 μm as the probe. The curve shows the theoretical fit for the free-carrier refraction (and absorption).

signal near zero delay (third-order response) is not optimized, and the signal from this nonlinearity is reduced. The ≈20% reduction in this signal is easily calculated from Eq. (10). The fits to the data discussed below take these effects into account. At relatively low irradiance, $\Delta T_{pv}(t_d)$ [Fig. 5(a)] consists of a peak near zero delay and a slow-decaying tail at longer delays, which lasts much longer than the laser pulse. The peak is due to nondegenerate bound electronic nonlinear refraction, as is evidenced by the fast response (i.e., the width is consistent with the width for CS_2, as is shown in Fig. 2).[12] This nonlinear refraction is determined to be negative from the relative positions of the peak and the valley. The slow-decaying tail comes from free-carrier refraction (also defocusing), at which the carriers are produced by degenerate 2PA of the excitation beam. As the irradiance increases, the relative value of the peak diminishes with respect to the long free-carrier tail. This occurs because the bound electronic effect is a third-order nonlinearity, whereas the two-photon-generated free-carrier nonlinearities result in an effective fifth-order nonlinearity.[2,3] Fitting the data shown in Fig. 5(a), we obtain $n_2^{xx}(\omega; 2\omega) = (9 \pm 5) \times 10^{-15}$ cm^2/W, $\sigma_r(\omega) = 5.4 \pm 1.5 \times 10^{-22}$ cm^3, and a carrier decay time of $\tau_r \simeq 1$ ns. The errors on n_2 are large as the nonlinearity is dominated by free-carrier refractive effects, and such a large difference between $n_2^{xx}(\omega;2$ and $n_2^{xx}(2\omega;\omega)\omega) = -(5.1 \pm 1.0) \times 10^{-4}$ cm^2/W is not expected from a two-parabolic-band model, which predicts values within ≈10% of each other.[12]

Figure 5(b) shows $T_{op}(t_d)$ for ZnSe, giving the time-resolved nondegenerate nonlinear absorption. At zero delay the nondegenerate 2PA dominates, and at longer time delays we see a small contribution from 2PA-generated free-carrier absorption. As stated above, the free-carrier refraction and absorption are proportional to the density of free carriers, which slowly decays with the recombination time τ_r of the carriers. The fit that is shown uses $\beta = 4.6 \pm 1.1$ cm/GW and $\sigma_a = (4.4 \pm 1.3) \times 10^{-1}$ cm^2.

Fixing the delay of the probe relative to the excitation beam so that the two pulses have no temporal overlap and performing a two-color Z scan, we see only free-carrier refraction and absorption. Experimental data, depicting the ratio of the closed-aperture to the open-aperture Z scans for ZnSe at 100 and 200-ps time delay (with $I_e = 1.5$ GW/cm^2), are shown in Fig. 6. Because a delay time of 200 ps is considerably less than τ_r, the number of free carriers is the same within 10% at the two delays. The free-carrier refraction, $\sigma_r(\omega) = 6 \pm 1.5 \times 10^{-22}$ cm^3, and absorption, $\sigma_a(\omega) = 4.4 \pm 1.3 \times 10^{-18}$ cm^2, from these Z scans are consistent with those obtained from the time-delay experiment to within 10%.

The data for ΔT_{pv} for ZnS, as shown in Fig. 7(a), display no fast-response signal near zero delay. This result indicates that the phase change produced by the free car-

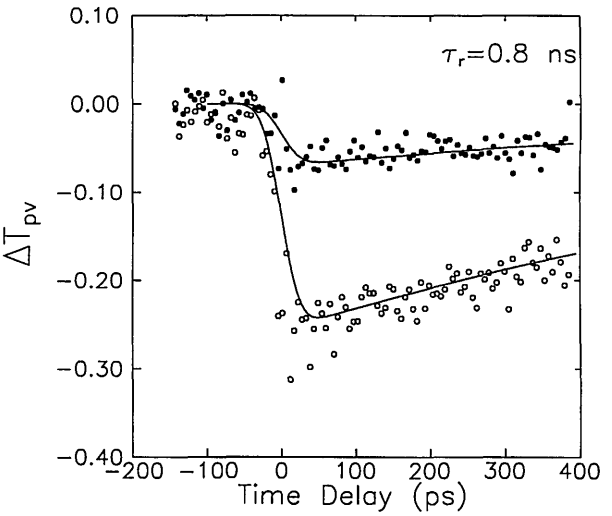

(a)

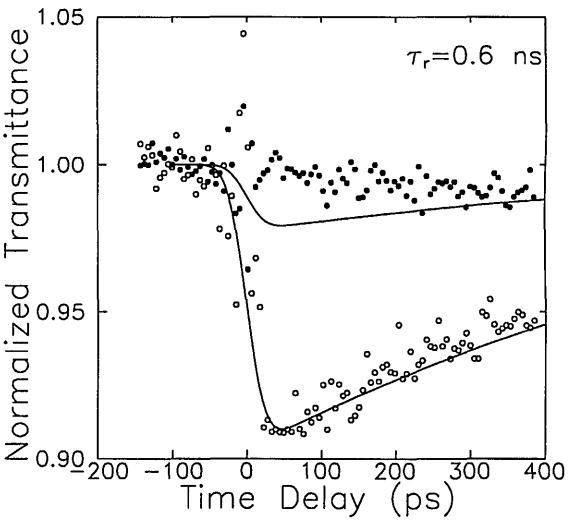

(b)

Fig. 7. (a) Nonlinear refraction as determined by ΔT_{pv} and (b) nonlinear absorption from the normalized transmittance T_{op} as a function of probe-beam time delay t_d for ZnS measured at $I_e = 0.7$ GW/cm^2 (filled circles) and $I_e = 1.45$ GW/cm^2 (open circles). The curves are fits to the data obtained with the values given in Table 1.

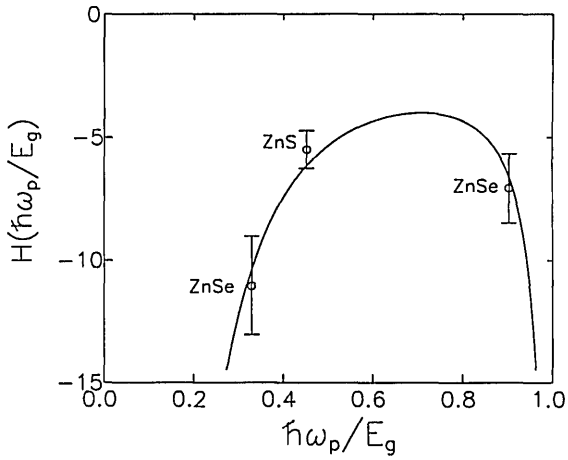

Fig. 8. Free-carrier nonlinear refraction as a function of probe-beam photon energy ($\hbar\omega_p/E_g$) for ZnS at 0.532 μm and for ZnSe at 1.06 and 0.532 μm.

riers is much larger than that produced by the bound electrons. In addition, based on the theory,[12] we expect the nondegenerate n_2 to be positive, partially negating the self-defocusing from the carriers. However, the free-carrier nonlinearities totally dominate the phase change at high irradiance, resulting in a good fit for ZnS by use of only carrier effects. The nonlinear absorption for ZnS, shown in Fig. 7(b), is dominated by free-carrier absorption because there is no nondegenerate 2PA. Note that, for both irradiances, at zero delay there is a narrow spike of unknown origin. We speculate that this result may be caused by transient beam coupling or by a cascading of second-order nonlinearities.[25]

We find that, from the higher irradiance data shown in Fig. 7 for ZnS, $\sigma_a(\omega) = 8 \pm 2 \times 10^{-18}$ cm^2 and $\sigma_r(\omega) = -5 \pm 1 \times 10^{-22}$ cm^3 (curves in Fig. 7). These two experiments give slightly different values for the carrier recombination time ($\tau_r \simeq 0.6$ ns for free-carrier absorption and $\tau_r \simeq 0.8$ ns for free-carrier refraction measurements). This small difference may be explained by the different relative contributions of free electrons and holes to refraction and absorption and by possible differences in electron- and hole-trapping rates.

C. Dispersion of Free-Carrier Nonlinearities

There exist numerous theoretical models dealing with the effects of an electron–hole plasma on the complex dielectric constant.[15–17] We find that the simplest model,[9,15,16] which incorporates two parabolic bands, sufficiently explains the magnitude and the dispersion of the observed free-carrier effects.[3] In this simple model the change of refractive index for wavelengths below the band edge (i.e., for probe photon energy $\hbar\omega_p < E_g$) that is due to an injection of an electron–hole density ΔN is given by[9,16]

$$\Delta n(\omega_p) = \frac{2\pi e^2 \Delta N}{m_{e\text{-}h}} \left(-\frac{1}{{\omega_p}^2} - \frac{1}{{\omega_g}^2 - {\omega_p}^2} \right), \qquad (12)$$

where $m_{e\text{-}h}$ is the electron–hole reduced effective mass and $\omega_g = E_g/\hbar$. The first term in Eq. (12) describes the Drude plasma contribution, and the second term represents the band-filling contribution to the refractive-index change. A more general expression can be obtained by elimination of the effective mass with the results of $\mathbf{k} \cdot \mathbf{p}$ theory[28]:

$$\frac{m_{e\text{-}h}}{m_0} \simeq \frac{E_g}{E_p}, \qquad (13)$$

where only the heavy-hole valence band is taken into account. Here $E_p \simeq 21$ eV is the Kane energy and is nearly material independent for most semiconductors.[28] This allows us to write Eq. (12) as

$$\Delta n(\omega_p) = A \frac{E_p}{n_0 {E_g}^3} H\left(\frac{\hbar\omega_p}{E_g}\right) \Delta N, \qquad (14)$$

where $H(x) = [x^2(x^2 - 1)]^{-1}$ is the free-carrier dispersion function and $A = 2\pi\hbar^2 e^2/m_0 = 3.4 \times 10^{-22}$ cm^3 eV^2. The advantage of Eq. (14) is that it provides a simple E_g scaling as well as a dispersion function that is only a function of $\hbar\omega/E_g$. This is analogous to the useful expressions derived for the bound electronic nonlinearities in semiconductors.[11,27] Under the quasi-equilibrium condition, the free-carrier effects are independent of the means of generation, and thus Δn has no explicit dependence on the excitation photon energy $\hbar\omega_e$.

A best fit to our experimental data for ZnSe and ZnS is obtained with $A \simeq 2.3 \times 10^{-22}$ cm^3 eV^2. We plot the dispersion function $H(\hbar\omega_p/E_g)$ and the experimental results in Fig. 8. The good agreement between our results and this simple model may exist in part because the carrier densities reached are relatively low, $\Delta N < 10^{18}$ cm^{-3}, and in part because we probe relatively far below the gap. At high carrier densities and at photon energies near the gap, many-body effects and excitons may become important.[17]

5. CONCLUSION

We have introduced a time delay for one of the beams in a two-color Z-scan apparatus to allow the temporal dependence of the nonlinear absorption and the nonlinear refraction to be separately measured. We have demonstrated the utility of this technique by monitoring the several nonlinearities that occur in semiconductors on a picosecond time scale. Whereas these nonlinearities normally require that several different types of experiments be performed to separate their similar effects, this new technique (temporally resolved two-color Z scan) permits their separation by itself. In particular, we have separately measured the nondegenerate two-photon absorption, bound electronic n_2, free-carrier absorption, and free-carrier refraction in ZnSe and have performed similar experiments on ZnS, for which nondegenerate two-photon absorption is not energetically permitted, and on CS_2, which shows only nonlinear refraction. The numerous parameters extracted from these data (see Table 1) have been compared with simple band-theory models that have been presented elsewhere. One can also extend this technique to obtain the temporal dependence of different nonlinear tensor components by changing the relative polarization of the excitation and the probe beams.

It may be of use to contrast this technique with DFWM at this point. Temporally resolved DFWM uses three interacting beams at the same wavelength to produce a

fourth beam whose energy can be measured as a function of the time delay of any one of the three beams, with the other two being fixed at zero delay. The absolute accuracy of determining a nonlinear coefficient with DFWM is expected to be considerably less than with the technique discussed in this paper because in DFWM three, as opposed to two, beams must be both accurately characterized (i.e., beam shape, pulse width, and energy) and overlapped spatially and temporally. In addition, the results of the DFWM experiment for third-order nonlinearities are proportional to $|\chi^{(3)}|^2$ such that absorptive and refractive contributions are mixed. However, temporal information and symmetry properties of the degenerate susceptibilities can be measured. On the other hand, decay is often governed by diffusion between fringes, which can be much faster than diffusion across the entire beam. As stated above, measuring degenerate nonlinearities with the time-resolved Z scan presents other difficulties. Therefore this new technique should be considered complementary to other experimental methods, such as DFWM, for determining the origins of optical nonlinearities of materials.

ACKNOWLEDGMENTS

We gratefully acknowledge the support of the National Science Foundation (grant ECS 9120590), the Defense Advanced Research Projects Agency, and the Night Vision and Electro-Optics Directorate.

REFERENCES

1. J. J. Wynne, "Optical third-order mixing in GaAs, Ge, Si, and InAs," Phys. Rev. **178,** 1295 (1969); see also P. Roussignol, D. Ricard, and C. Flytzanis, "Nonlinear optical properties of commercial semiconductor doped glasses," Appl. Phys. A **44,** 285 (1987).
2. E. Canto-Said, D. J. Hagan, J. Young, and E. W. Van Stryland, "Degenerate four wave mixing measurements of higher order nonlinearities in semiconductors," IEEE J. Quantum Electron. **27,** 2274 (1991).
3. A. A. Said, M. Sheik-Bahae, D. J. Hagan, T. H. Wei, J. Wang, J. Young, and E. W. Van Stryland, "Determination of bound-electronic and free-carrier nonlinearities in ZnSe, GaAs, CdTe, and ZnTe," J. Opt. Soc. Am. B **9,** 405 (1992).
4. H. Ma, A. S. L. Gomes, and C. B. de Araujo, "Measurement of nondegenerate optical nonlinearity using a two-color single beam method," Appl. Phys. Lett. **59,** 2666 (1991).
5. J. Sheik-Bahae, J. Wang, R. DeSalvo, D. J. Hagan, and E. W. Van Stryland, "Measurement of nondegenerate nonlinearities using a two-color Z scan," Opt. Lett. **17,** 260 (1992).
6. M. Sheik-Bahae, A. A. Said, and E. W. Van Stryland, "High-sensitivity, single-beam n_2 measurements," Opt. Lett. **14,** 955 (1989).
7. M. Sheik-Bahae, A. A. Said, T. H. Wei, D. J. Hagan, and E. W. Van Stryland, "Sensitive measurement of optical nonlinearities using a single beam," IEEE J. Quantum Electron. **26,** 760 (1990).
8. E. W. Van Stryland, H. Vanherzeele, M. A. Woodall, M. J. Soileau, A. L. Smirl, S. Guha, and T. F. Boggess, "Two-photon absorption, nonlinear refraction, and optical limiting in semiconductors," Opt. Eng. **24,** 613 (1985).
9. D. H. Auston, S. McAffee, C. V. Shank, E. P. Ippen, and O. Teschke, "Picosecond spectroscopy of the semiconductors," Solid-State Electron. **21,** 147 (1978).
10. E. W. Van Stryland, A. L. Smirl, T. F. Boggess, M. J. Soileau, B. S. Wherrett, and F. Hopf, "Weak-wave retardation and phase-conjugate self-defocusing in Si," in *Picosecond Phenomena III,* K. B. Eisenthal, R. M. Hochstrasser, W. Kaiser, and A. Laubereau, eds. (Springer-Verlag, New York, 1982), p. 368.
11. M. Sheik-Bahae, D. J. Hagan, and E. W. Van Stryland, "Dispersion and band-gap scaling of the electronic Kerr effect in solids associated with two-photon- absorption," Phys. Rev. Lett. **65,** 96 (1989).
12. M. Sheik-Bahae, D. C. Hutchings, D. J. Hagan, and E. W. Van Stryland, "Dispersion of bound electronic nonlinear refraction in solid," IEEE J. Quantum Electron. **27,** 1296 (1991).
13. D. C. Hutchings, M. Sheik-Bahae, D. J. Hagan, and E. W. Van Stryland, "Kramers–Kronig relations in nonlinear optics," Opt. Quantum Electron. **24,** 1 (1992).
14. F. Bassani and S. Scandolo, "Dispersion relations and sum rules in nonlinear optics," Phys. Rev. B **44,** 8446 (1991).
15. D. A. B. Miller, C. T. Seaton, M. E. Prise, and S. D. Smith, "Band-gap-resonant nonlinear refraction in III–V semiconductors," Phys. Rev. Lett. **47,** 197 (1981).
16. A. G. Aronov, D. E. Pikus, and D. Sh. Shekhter, "Quantum theory of free-electron dielectric constant in semiconductors," Sov. Phys. Solid State **10,** 645 (1968).
17. L. Banyai and S. W. Koch, "A simple theory for the effects of the plasma screening on the optical spectra of highly excited semiconductors," Z. Phys. B **63,** 283 (1986).
18. R. Luzzi and A. R. Vasconcellos, "Relaxation processes in nonequilibrium semiconductor plasma," in *Semiconductors Probed by Ultrafast Laser Spectroscopy,* R. R. Alfano, ed. (Academic, New York, 1984), Vol. 1.
19. J. I. Pankove, *Optical Processes in Semiconductors* (Prentice-Hall, Englewood Cliffs, N.J., 1971).
20. S. A. Akmanov, R. V. Khokhlov, and A. P. Sukhorukov, "Self-focusing, self-defocusing, and self-modulation of laser beams," in *Laser Handbook,* F. T. Arecchi and E. O. Schultz-Dubois, eds. (North-Holland, Amsterdam, 1972), Vol. 2, p. 1151.
21. H. A. Haus, *Waves and Fields in Optoelectronics* (Prentice-Hall, Englewood Cliffs, N.J., 1984).
22. J. D. Gaskill, *Linear Systems, Fourier Transforms, and Optics* (Wiley, New York, 1978).
23. J. Wang, "The dispersion and symmetry of optical nonlinearities in semiconductors," Ph.D. dissertation (University of Central Florida, Orlando, Florida, 1993).
24. B. Ray, *II–VI Compounds* (Pergamon, Edinburgh, 1969), Chap. 6.
25. R. J. DeSalvo, D. J. Hagan, M. Sheik-Bahae, G. Stegeman, E. W. Van Stryland, and H. Vanherzeele, "Self-focusing and self-defocusing by cascaded second-order effects in KTP," Opt. Lett. **17,** 28 (1992).
26. M. Sheik-Bahae, J. Wang, E. J. Canto-Said, R. DeSalvo, D. J. Hagan, and E. W. Van Stryland, "Two-photon coherence and symmetry of $\chi^{(3)}$ in semiconductors," in *Quantum Electronics and Laser Science Conference,* Vol. 12 of 1993 OSA Technical Digest Series (Optical Society of America, Washington, D.C.), paper QTuK26.
27. M. Sheik-Bahae, J. Wang, and E. Van Stryland, "Nondegenerate optical Kerr effect in semiconductors," IEEE J. Quantum Electron. (to be published).
28. E. O. Kane, "Band structure of indium antimonide," J. Chem. Phys. **1,** 249 (1957).